Sulfur−Gold Orbital Interactions which Determine the Structure of Alkanethiolate/Au(111) Self-Assembled Monolayer Systems

Masamitsu Tachibana,[†,‡] Kazunari Yoshizawa,[*,†] Atsushi Ogawa,[‡] Hiroshi Fujimoto,[*,‡] and Roald Hoffmann[*,§]

Institute for Fundamental Research of Organic Chemistry, Kyushu University, Fukuoka 812-8581, Japan, Department of Molecular Engineering, Kyoto University, Kyoto 606-8501, Japan, and Department of Chemistry and Chemical Biology, Cornell University, Ithaca, New York 14853-1301

Received: April 17, 2002; In Final Form: August 3, 2002

With the aim of understanding the nature of the S−Au(111) bonding in organosulfur/Au(111) self-assembled monolayer (SAM) systems, orbital interactions in the adsorption of methanethiolate ($^{-}SCH_3$) in various binding sites of a three-layer slab model and an Au_{42} cluster model of Au(111) surface are investigated. The methods of choice are crystal orbital overlap population (COOP) and crystal orbital Hamilton population (COHP) analyses for a periodic slab model and fragment molecular orbital (FMO) analyses for the cluster model. The origin of the S−Au(111) bond and the binding site preference are discussed from the viewpoint of orbital interaction. The site preference is in the order of three-fold hollow (*fcc* and *hcp*) > bridge > on-top. The second layer Au atoms have little influence on the S−Au(111) bonding, and adsorptions to the *fcc* and *hcp* sites are almost identical with respect to energy and S−Au bonding nature. Although σ-type S−Au orbital interactions dominate the S−Au(111) bonding in the on-top model, π-type S−Au orbital interactions play an important role in the bridge, *fcc*, and *hcp* models. FMO results explain the vertical S−C bonds in the hollow models and the tilted S−C bonds in the on-top and bridge models.

1. Introduction

Self-assembled monolayers (SAMs) have attracted much attention because of their unique highly ordered structures and potential applications to nanofabrications and chemical sensing.[1] Monolayers of alkanethiols ($CH_3(CH_2)_nSH$) or dialkyl disulfides ($CH_3(CH_2)_nS-S(CH_2)_nCH_3$) on the Au(111) surface have been most widely studied owing to their simplicity, chemical stability, and easy preparation.[2] Despite the extensive practical utilization of these SAMs, fundamental aspects of the organosulfur monolayers on Au(111), including the nature of the S-surface interaction, are still under debate and are not well understood.

In the self-assembly process of the organosulfur/Au(111) systems, a low-density phase is initially formed by rapid adsorption of sulfur-containing molecules, followed by slow evolution to a full-coverage high-density phase.[3] Several different phases are observed during the evolution. The adsorbates "lie down" on the surface in a low-density phase, whereas they "stand up" in a high-density phase. The structures of the monolayers are widely considered to be determined by a balance between the headgroup-surface (S−Au) interaction as well as the dispersion force (van der Waals interaction) between the alkyl chains. The contribution of the dispersion forces would be dominant in a high-density phase formed by long-chain adsorbates. Interestingly, the final adsorption phases of alkanethiols and dialkyl disulfides have been reported to be identical,[4] which raises the question whether the adsorbed species are thiolate or disulfide.

From measurements of X-ray photoelectron spectroscopy (XPS), Auger electron spectroscopy (AES), high-resolution electron energy loss spectroscopy (HREELS), and thermal desorption spectroscopy (TDS), Nuzzo et al. suggested that the S−S bond of dimethyl disulfide cleaves to form two methanethiolate−surface bonds.[5] For long-chain alkanethiolate monolayers, electron[6] and helium diffraction (HeD)[7] studies revealed that the high-density phase is a commensurate ($\sqrt{3} \times \sqrt{3}$)-R30° lattice of thiolates with an S−S distance of ∼5 Å. The proposed ($\sqrt{3} \times \sqrt{3}$)R30° structure has been confirmed by grazing incidence X-ray diffraction (GIXD),[8] molecular dynamics (MD) simulation,[9] and scanning tunneling microscopy (STM).[10]

Thus, it is widely accepted that the surface−adsorbate bonding is in the form of Au-thiolate. The S headgroups are believed to occupy the three-fold hollow sites, although there is no direct information about the binding site.[4c,6,7,10,11] Ishida et al.[12] and Noh and Hara[13] recently observed phase-separated domains in the SAMs of asymmetric disulfides and confirmed dissociative adsorption of disulfides. The formation of the Au−thiolate bond starting from alkanethiol and dialkyl disulfide can be written as follows:

$$RS - H + Au_n^0 \rightarrow RS - Au + Au_n^0 + 1/2H_2$$

$$RS - SR + Au_n^0 \rightarrow RS - Au + Au_n^0$$

The ($\sqrt{3} \times \sqrt{3}$)R30° model was challenged by a HeD experiment,[14] which reported that the high-density phase is not the simple ($\sqrt{3} \times \sqrt{3}$)R30° structure but a c(4 × 2) superlattice of the ($\sqrt{3} \times \sqrt{3}$)R30° overlayer. The c(4 × 2) superlattice structure was supported by GIXD,[15] X-ray standing wave (XSW),[16] and scanning probe microscopy (SPM) measure-

* To whom correspondence should be addressed. E-mail: kazunari@ms.ifoc.kyushu-u.ac.jp (K.Y.); lavender@zeus.eonet.ne.jp (H.F.); rh34@cornell.edu (R.H.).
† Kyushu University
‡ Kyoto University
§ Cornell University

10.1021/jp020993i CCC: $22.00
Published on Web 11/14/2002

ments.[17] Fenter et al. pointed out from a multiparameter analysis of GIXD data[18] that the S atoms in the c(4 × 2) superlattice are located in different sites and S-headgroup dimers are formed with an S−S distance of 2.2 Å. Therein, they noted that, in the limit of small chain length, the high-density phase may adopt the ($\sqrt{3} \times \sqrt{3}$)R30° structure (therefore, the adsorbed species are thiolates) because the S-surface interaction is dominant over interchain interactions. The S−S bonding model for long-chain adsorbates is further supported by results of sum-frequency generation (SFG),[19] HREELS,[20] and MD simulation.[21]

To elucidate the adsorption state, several theoretical studies have been carried out. Sellers et al. first performed ab initio geometry optimizations of SH and SCH_3 on cluster models of Au(111) surface and showed definite preference for the hollow site.[22] Beardmore et al. suggested that the SCH_3 adsorption to the *fcc*, *hcp*, and bridge sites are isoenergetic and thiolates can easily diffuse on Au(111) surface,[23] where both *fcc* and *hcp* sites are three-fold hollow sites. The difference is that the *hcp* site has a second-layer gold atom just below the site, whereas the *fcc* site does not. From a full relaxation study for Au_{38}-(CH_3S-SCH_3), Häkkinen et al. recently reported that molecular adsorption of dimethyl disulfide is energetically unfavorable compared to dissociative adsorption to the two nonadjacent bridge sites.[24] The problem of whether the stable adsorption state is thiolate-like or disulfide-like was also theoretically studied by Grönbeck et al.,[25] Hayashi et al.,[26] and Selloni et al.[27] They agreed in supporting dissociative adsorption of dimethyl disulfide but reached different conclusions about the binding site of methanethiolate. Grönbeck et al. proposed that the preferred site is the *fcc* site,[25] which was supported by Yourdshahyan et al.,[28] who examined *n*-alkanethiolate monolayers on a slab model for several alkyl chain lengths and coverages. According to Selloni et al., adsorption at the bridge site is by far the most stable for a range of coverage.[27] Hayashi et al. suggested that the most preferred site for methanethiolate is not one of the highly symmetric sites but a bridge site slightly off-centered toward the *fcc* site.[26] Hirao et al. also found from theoretical calculations including relativistic effects[29] that methanethiolate is accommodated in a position between the bridge and *fcc* sites,[30] being consistent with the result by Gottschalck and Hammer.[31]

Thus, experimental and theoretical studies on the adsorption state in the organosulfur/Au(111) systems vary significantly in their conclusions. The theoretical investigations mentioned above are mainly based on the comparison of total energies of various possible adsorbed structures. The numbers may be there (not that they agree), but the nature of the bonding of the S−Au interface is still unclear. We feel it is important to clarify the essential features of the S-surface bonding and site preferences for adsorption.

Our main focus in this work is the S-surface bonding in the organosulfur/Au(111) systems. We calculated and analyzed methanethiolate ($^-SCH_3$) adsorption to a three-layer slab model and an Au_{42} cluster model of Au(111) at the extended Hückel level of theory.[32] We carried out crystal orbital overlap population (COOP)[33] and crystal orbital Hamilton population (COHP)[34] analyses for the slab model and fragment molecular orbital (FMO)[35] analyses for the cluster model, so as to illuminate the orbital interactions that play a role in the S-surface bonding.

2. COOP and COHP Analyses

2.1. Slab Model. The clean Au(111) surface shows a ($\sqrt{3} \times 23$) reconstruction[36] known as "herringbone structure" to obtain higher atomic density. However, because the reconstruction reverts to the bulk structure during an adsorption process,[3a,d,19] we do not consider the surface reconstruction in the present study. We approximated the Au(111) surface by a three-layer slab with the nearest Au−Au distance of 2.884 Å,[2c,3e,22,23b,37] the value for bulk gold. One of the two surfaces of the slab is covered with a monolayer of methanethiolate ($^-SCH_3$). The total charge of the monolayer/slab model was fixed to be zero. This model can be viewed as a model for the adsorption of SCH_3 radicals to the neutral gold slab. For clarity, we assumed the arrangement of $^-SCH_3$ overlayer to be simple ($\sqrt{3} \times \sqrt{3}$)R30°, with the S headgroups being bound to equivalent high-symmetry sites (on-top, bridge, *fcc*, or *hcp*). Thus, we considered four kinds of adsorption models, on-top, bridge, *fcc*, and *hcp*. Figure 1 shows the unit cell of the two-dimensional model containing one $^-SCH_3$ and nine Au atoms (three Au atoms in each layer) along with a schematic representation of the ($\sqrt{3} \times \sqrt{3}$)R30° overlayer. Because the S-surface distance, S−C bond length, and Au−S−C bond angle will significantly influence the S-surface orbital interaction, we should be careful in determining these geometrical parameters.

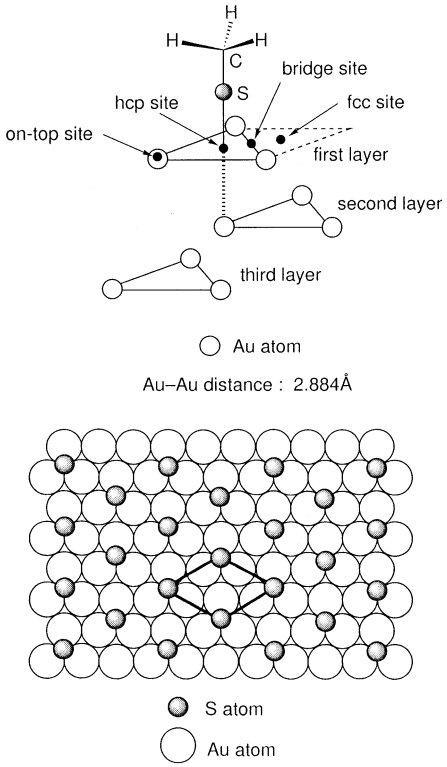

Figure 1. Above: the unit cell of a slab model of the *hcp* adsorption. Below: a schematic representation of a ($\sqrt{3} \times \sqrt{3}$)R30° overlayer of methanethiolate. For clarity, only the surface Au atoms and the S atoms are shown. The S atoms are assumed to occupy equivalent three-fold hollow sites. The bold line indicates the unit mesh.

There are several state-of-the-art geometry optimizations of methanethiolates on Au(111).[22−28,30,31] Therefore, we can use the results of previous theoretical studies. We mainly employed the optimized geometries of Hirao et al.;[30] see Figure 2. They calculated one SCH_3 on a two-layer Au_{18} cluster model of Au(111) at the BLYP[38] level of density-functional theory (DFT), employing periodic boundary conditions. They used a numerical basis set whose quality corresponds to the valence-double-ζ and polarization levels. Relativistic effects were included in the geometry optimizations with the DMOL3 ver. 4.0 program.[39] They systematically provided optimized geometrical parameters for the SCH_3 moiety including S−C bond length and Au−S−C

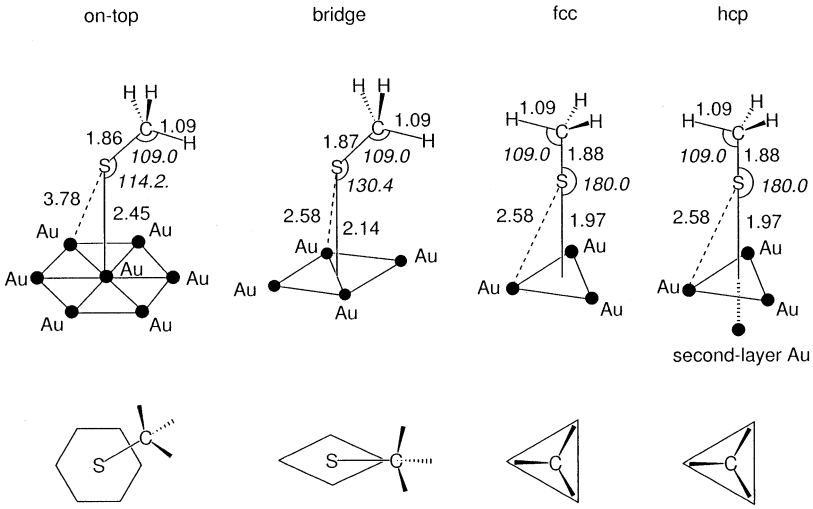

Figure 2. Geometries used in the extended Hückel calculations. All of the Au−Au distances are fixed to 2.884 Å. Bond lengths are in Å, and bond angles are in degree.

bond angle for the three kinds of adsorption sites, on-top, bridge, and three-fold hollow (*fcc*), which lacks in most theoretical studies.[22−28] Therefore, the paper of Hirao et al. is adequate to obtain consistent geometrical information about the SCH_3 moiety for the three kinds of sites. The optimized S-surface distances for the on-top, bridge, *fcc*, and *hcp* sites are 2.45, 2.14, 1.97, and 1.97 Å, respectively. To see the influence of the second layer, we assumed the same SCH_3 structures for the *fcc* and *hcp* sites. Although previous theoretical studies on the SCH_3/Au(111) systems predicted somewhat different S-surface distances, relative values of the S-surface separations for the highly symmetric sites are on-top > bridge > three-fold hollow in most cases.[22,25−28,30,31] We see in Figure 2 that the S−C bonds are vertical to the Au(111) surface for the hollow site adsorptions. This is consistent with previous theoretical predictions[22,25] and our DFT calculations using small Au clusters. The underlying reason for the vertical S−C bonds will be explained later in this paper. We assumed all of the C−H distances and the S−C−H angles to be 1.09 Å and 109°, respectively. This assumption is reasonable, because a small geometrical change within the CH_3 moiety will have little influence on the S-surface interaction. We also tested 6- and 10-layer slabs for the on-top case, but the main features of the S-surface interactions were essentially identical to those obtained with the three-layer slab. Thus, we think that our three-layer slab models are appropriate for crystal orbital overlap population (COOP) and crystal orbital Hamilton population (COHP) analyses.

2.2. Theoretical Background. We carried out crystal orbital overlap population (COOP) and crystal orbital Hamilton population (COHP) analyses to investigate and rationalize the S−Au(111) bonding interaction. Although COOP and COHP are based on simple approximations, they can be directly related to chemical intuition and are useful in understanding the origin of chemical bonds.

The COOP method is an electron partitioning scheme for extended systems, which provides information about electron distribution. All of the COOP terms can be classified into "on-site" COOP terms and "off-site" COOP terms.[34] On- and off-site COOP terms sum up to the total number of electrons of a unit cell, and an off-site COOP term denotes electron distribution to an overlap between two different atomic orbitals (AOs). A positive off-site COOP value indicates bonding interaction (in-phase overlap) of two AOs and strengthening of the chemical bond between the atoms concerned, whereas a negative value means the opposite. Off-site COOP between μth atomic orbital of "home cell" and νth atomic orbital of the cell represented by lattice vector R is given by eq 1:

$$\mathrm{COOP}_{\mu\nu}(R) = \sum_{k\in K} \Omega_k \sum_{\substack{\mathrm{CO's}\\ i}} n_i(k)\{C^*_{\mu i}C_{\nu i}e^{ikR} + C_{\mu i}C^*_{\nu i}e^{-ikR}\}S_{\mu\nu}(R) \quad (1)$$

Here Ω_k is the weighting of a reciprocal space point k belonging to the discrete set K, and $n_i(k)$ is crystal orbital (CO) occupation of ith CO. AO coefficients for the AOs μ and ν are represented by $c_{\mu i}$ and $c_{\nu i}e^{ikR}$, respectively, and $S_{\mu\nu}(R)$ is the overlap integral for the two AOs. For simplicity, we can group COOP terms based on atoms or molecular fragments. If we group COOPs by atoms, all of the COOP terms are recast into on- and off-site atomic terms (intra- and interatomic terms). These correspond to the numbers of electrons distributed to atoms and chemical bonds, respectively. Therefore, we can relate interatomic COOPs to "bond orders". Using the COOP analysis, we can estimate the strength of orbital interaction (bond order) between the S headgroup and Au(111) surface as well as the contribution from each AO pair.

The COHP formalism is a total energy partitioning scheme for extended systems. COHP is described as an "energy weighted" COOP. The COHP method enables us to distribute the total electronic energy to atoms and bonds. Here, off-site interatomic COHP values can be regarded as "bond energies". We can divide the interatomic COHP into contributions from pairs of valence AOs. With the COHP analysis, we can directly attribute the difference in S−Au binding energy among possible adsorbed structures to certain AO interactions. The off-site COHP term corresponding to eq 1 is written as eq 2 employing the Wolfsberg−Helmholz approximation:[40]

$$\mathrm{COHP}_{\mu\nu}(R) = \sum_{k\in K} \Omega_k \sum_{\substack{\mathrm{CO's}\\ i}} n_i(k)\{C^*_{\mu i}C_{\nu i}e^{ikR} + C_{\mu i}C^*_{\nu i}e^{-ikR}\}\frac{1.75}{2}(H_{\mu\mu} + H_{\nu\nu})S_{\mu\nu}(R) \quad (2)$$

where $H_{\mu\mu}$ and $H_{\nu\nu}$ are diagonal Hamilton matrix elements, which are related to valence shell ionization potentials of the μth and νth AOs. It should be noted that a negative off-site COHP term represents bonding interaction, corresponding to a positive COOP term.

TABLE 1: Atomic Parameters Used in the Extended Hückel Calculations

atom	orbital	H_{ii} (eV)	ζ_1	c_1	ζ_2	c_2
Au	6s	−10.92	2.602			
	6p	−5.55	2.584			
	5d	−15.07	6.163	0.6442	2.7940	0.5356
S	3s	−20.00	2.122			
	3p	−11.00	1.827			
C	2s	−21.40	1.625			
	2p	−11.40	1.625			
H	1s	−13.60	1.300			

SCHEME 1

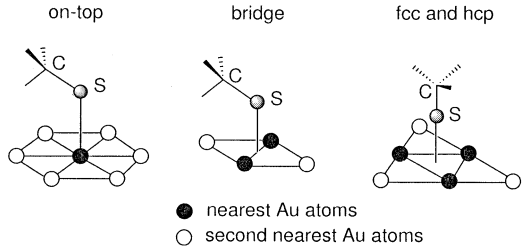

2.3. Computational Details. We performed band calculations on methanethiolate monolayers on the three-layer Au(111) slab at the extended Hückel level, using the YAeHMOP[41] program. A 45 k point set was used to calculate COOP and COHP terms. The atomic parameters used in the extended Hückel calculations are listed in Table 1. H_{ii}, ζ, and c are orbital energy, Slater exponent, and coefficient, respectively. To understand the essence of S−Au(111) bonding and explain the site preference, we carried out COOP and COHP analyses for the S−Au interface. We confirmed that the neighboring parts such as the second Au layer has little influence on the S-surface interaction. We first calculated the interatomic COOPs and interatomic COHPs of the S-nearest Au atoms and S-second-nearest Au atoms in each adsorbed structure. These values can be directly related to the strength of the S-surface bonding. The nearest and second-nearest Au atoms are indicated by black circles and white circles in Scheme 1, respectively. To further investigate the S−Au interaction, we calculated off-site COOPs and off-site COHPs between the valence AOs of the S atom and those of the nearest Au atoms. That is, the 4 × 9 interactions between the 3s, $3p_x$, $3p_y$, and $3p_z$ orbitals of the S atom and the 6s, $6p_x$, $6p_y$, $6p_z$, $5d_{x^2-y^2}$, $5d_{z^2}$, $5d_{xy}$, $5d_{xz}$, and $5d_{yz}$ orbitals of the nearest Au atoms are considered. This AO based analysis will be helpful to elucidate the essence of the S−Au orbital interactions.

2.4. Results and Discussion. We list in Table 2 the distances and total interatomic COOPs and total interatomic COHPs between the S atom and the nearest Au atoms and between the S atom and the second-nearest Au atoms. We also present the total COOPs and total COHPs for the nearest and the second-nearest S−Au bonds. Table 2 shows that the S-surface bonding is dominated by the nearest S−Au interactions and the contributions of the second-nearest Au atoms are very small. This is reasonable, because the second-nearest S−Au distances are larger than the nearest S−Au separations by about 1 Å. Although the S-nearest Au interactions are all bonding, the interactions between the S atom and the second-nearest Au atoms are antibonding except in the bridge model.

The relative strength of the S-surface bonding is in the order three-fold hollow (*fcc* and *hcp*) > bridge > on-top. The similarity between the *fcc* and *hcp* adsorptions indicates that the second-layer Au atoms do not significantly affect the S-surface interaction. In the hollow models, total COOPs and total COHPs between the S atom and Au(111) are about +0.9 and −16.5 eV, respectively. In the bridge and on-top adsorptions, COOPs and COHPs for the S−Au(111) are smaller (+0.683 and −12.59 eV for the bridge model and +0.436 and −8.20 eV for the on-top model), and therefore, the S-surface binding is weaker in these models. As expected, the interatomic COHPs are nearly proportional to the corresponding interatomic COOPs. Although the absolute values of the total COHPs (∼16.5 eV = ∼380 kcal/mol) are too large to directly relate to an experimental desorption energy (40 ± 5 kcal/mol),[3d] we believe the relative values obtained and the characterizations of the bonding are qualitatively correct.

TABLE 2: Distances, Interatomic COOPs, and Interatomic COHPs for the Nearest and the Second-Nearest S−Au

model	S−Au distance/Å	S−Au COOP	S−Au COHP/eV
on-top	2.45	0.446	−8.52
	(3.78)[a]	(−0.010)	(0.32)
		0.436[b]	**−8.20**
bridge	2.58	0.660	−12.29
	(3.29)	(0.023)	(−0.30)
		0.683	**−12.59**
fcc	2.58	0.901	−16.71
	(3.87)	(−0.005)	(0.14)
		0.896	**−16.57**
hcp	2.58	0.904	−16.68
	(3.87)	(−0.006)	(0.17)
		0.898	**−16.51**

[a] Values for the second-nearest S−Au are given in parentheses. [b] Total values for the first- and second-nearest S−Au are shown by bold letters. [c] Positive COOP and negative COHP indicate bonding interaction. [d] Distances are in Å, COHPs are in eV, and COOPs are dimensionless.

We show in Table 3 the off-site COHPs obtained for the AO pairs between the S atom and the nearest Au atoms. In Table 3 parts 3.2, 3.3, and 3.4, the total values for the equivalent S−Au bonds are given in each cell (the three S−Au bonds for the *fcc* and *hcp* models and the two S−Au bonds for the bridge model). The COHPs concerning the 5d orbitals are summarized as 5d-(total) for each valence orbital of the S atom. We can estimate from Table 3 which S−Au valence AO interaction is dominant in each model. The 5d(Au) orbitals interact weakly with the valence orbitals of the S atom and do not contribute significantly to the S-surface bond. On the other hand, the interactions between the 3s(S) or 3p(S) orbitals and the 6s(Au) or 6p(Au) orbitals are relatively large, and in particular, the 3s(S)−$6p_z$-(Au) and 3p(S)−6s(Au) interactions play a dominant role in each model. All of the AO pairs consisting of the s and p orbitals have positive COOPs (negative COHPs) and therefore strengthen the S-surface bond. This is the reason that the nearest S−Au interactions contribute significantly to the S-surface bond. We present in Figure 3 schematic representations of the orbital interactions that afford the largest negative COHPs (indicated by bold characters in Table 3).

In the on-top adsorption, the σ-type $3p_z$(S)−6s(Au) interaction (type 1) is by far the most dominant. Types 2 and 3 are also σ-type interactions, and the COHPs of types 1−3 add up in total to 92% of the total S-surface COHP. Hence, the nature of the on-top bonding derives almost entirely from these σ-type interactions, with this being consistent with the results from previous studies.[22,30] Though there exist π-type interactions such as $3p_x$(S)−$6p_x$(Au) and $3p_y$(S)−$6p_y$(Au), their contributions are very small. Because of symmetry, the on-top model has many orthogonal AO pairs that do not affect the S-surface bonding (shown by — in Table 3.1). This is a reason for the weak S-surface bonding in the on-top model, taking into account that all of the AO pairs except those concerning 5d(Au) orbitals strengthen the S−Au bonds. The result of overlap population

TABLE 3: Off-Site COOPs and Off-Site COHPs for Valence AO Pairs of the Nearest S−Au

	Au6s	Au6p_x	Au6p_y	Au6p_z	Au5d(total)
			3.1. On-Top		
S3s	0.031	—[b]	—	0.067	−0.007
	(−0.88)[a]			**(−1.72)**[c]	(0.21)
S3p_x	—	0.011	—	—	−0.003
		(−0.16)			(0.08)
S3p_y	—	—	0.015	—	−0.007
			(−0.23)		(0.16)
S3p_z	0.193	—	—	0.138	0.008
	(−3.69)			**(−2.11)**	(−0.18)
			3.2. Bridge		
S3s	0.031	0.018	—	0.063	−0.008
	(−0.88)	(−0.46)		(−1.60)	(0.23)
S3p_x	0.142	0.006	—	0.131	−0.012
	(−2.73)	(−0.10)		**(−2.00)**	(0.28)
S3p_y	—	—	0.006	—	−0.007
			(−0.09)		(0.16)
S3p_z	0.159	0.045	—	0.079	0.007
	(−3.04)	(−0.69)		(−1.21)	(−0.16)
			3.3. *fcc*		
S3s	0.057	0.018	0.015	0.086	−0.015
	(−1.61)	(−0.47)	(−0.38)	**(−2.19)**	(0.46)
S3p_x	0.145	0.013	0.012	0.113	−0.018
	(−2.78)	(−0.20)	(−0.19)	(−1.72)	(0.41)
S3p_y	0.130	0.013	0.011	0.118	−0.015
	(−2.49)	(−0.19)	(−0.17)	(−1.81)	(0.35)
S3p_z	0.106	0.025	0.022	0.064	0.001
	(−2.03)	(−0.38)	(−0.33)	(−0.97)	(−0.02)
			3.4. *hcp*		
S3s	0.057	0.019	0.015	0.086	−0.015
	(−1.61)	(−0.47)	(−0.39)	**(−2.18)**	(0.46)
S3p_x	0.147	0.014	0.012	0.114	−0.019
	(−2.75)	(−0.21)	(−0.19)	(−1.74)	(0.44)
S3p_y	0.129	0.013	0.012	0.119	−0.016
	(−2.47)	(−0.20)	(−0.18)	(−1.82)	(0.37)
S3p_z	0.106	0.025	0.022	0.063	0.001
	(−2.02)	(−0.38)	(−0.34)	(−0.97)	(−0.03)

[a] COHPs are given in parentheses (in eV). [b] Several AO pairs have no interaction (shown by —). [c] The three largest negative COHPs are indicated by bold letters.

analysis for the on-top adsorption by Hirao et al.[30] is similar to our results listed in Table 3.1.

In the bridge model, the σ-type 3p_z(S)−6s(Au) interaction (type 1) is most important as in the on-top model. However, the π-type 3p_x(S)−6s(Au) and 3p_x(S)−6p_z(Au) interactions (types 2 and 3) also contribute much, which is a significant difference from the on-top model. The ratio of the COHPs of the types 2 and 3 interactions sum up to 38%, being larger than 24% of the 3p_z(S)−6s(Au) (type 1) interaction. Therefore, the bonding state in the bridge adsorption is characterized by a mixture of π- and σ-type interactions involving the two nearest Au atoms. The bridge model also has some orthogonal AO pairs, but the number of such pairs is smaller than that in the on-top model (6 and 10 pairs for the bridge and the on-top models, respectively). We can explain from these results the stronger $^-$SCH$_3$ binding to the bridge site.

Parts 3.3 and 3.4 of Table 3 are very similar, showing essentially identical bonding character of the *fcc* and *hcp* adsorptions. In both hollow-site adsorptions, the S-surface bonds are mainly characterized by π-type 3p_x(S)−6s(Au) (type 1) and 3p_y(S)−6s(Au) (type 2) interactions. Types 1 and 2 are considered to be two-fold degenerate pairs, and the COHPs of the two pairs total −5.27 eV (32%). Type 3 (σ-type interaction) in the hollow model is related to type 3 in the on-top model. We find in parts 3.3 and 3.4 of Table 3 that other π-type degenerate pairs (3p_x(S)−6p_z(Au) and 3p_y(S)−6p_z(Au)) also have significant contributions (COHP = −1.72 and −1.81 eV, respectively, in the *fcc* case). Thus, compared to the bridge model, π bonding is stronger in the hollow models. The prevailing π character in the hollow models are qualitatively supported by other theoretical studies.[22,30] Because the hollow models have no orthogonal AO pairs, every AO pair composed of the s and p orbitals strengthens the S−Au bond. Accordingly, it is reasonable that the hollow models show the strongest S-surface bonding.

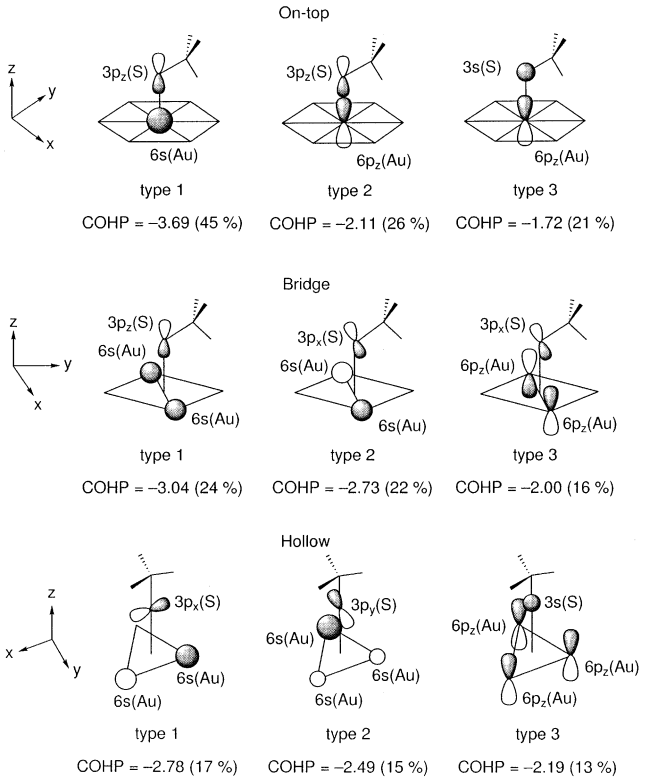

Figure 3. Schematic representations of the valence AO interactions between the S atom and the nearest Au atoms which have the largest negative COHPs. COHPs are in eV. We show in parentheses the ratio of each COHP (percentage) to the total S−Au COHP (in bold in Table 2). In the pictures of the hollow models, COHP values for *fcc* adsorption are presented.

As mentioned above, the π-type degenerate pairs (types 1 and 2) contribute considerably to the S-surface bonding. Because degenerate 3p_x(S) and 3p_y(S) orbitals are needed to afford these π-type interactions, the S headgroup should adopt "sp" hybridization.[22] This is a reason for the S−C bonds to be perpendicular to the Au(111) surface in the hollow models.

Summarizing the COOP and COHP analyses, the binding site preference for the $^-$SCH$_3$ adsorption to Au(111) surface is three-fold hollow (*fcc* and *hcp*) > bridge > on-top. The results of AO based COOP and COHP analyses (Table 3 and Figure 3) clarified the origin of the S−Au bond and explained the above site preference. The *fcc* and *hcp* adsorptions are almost indistinguishable in bonding nature. The π character of the S−Au(111) bond also decreases in the order, three-fold hollow > bridge > on-top. The strong π-type bonding interactions in the hollow models lead to the vertical S−C bonds in Figure 2.

3. FMO Analysis

3.1. Theoretical Background. It is useful to approach the problem of S−Au(111) bonding from a different perspective. To do this, we performed fragment molecular orbital (FMO) calculations to analyze the S−Au interactions and tilting angles

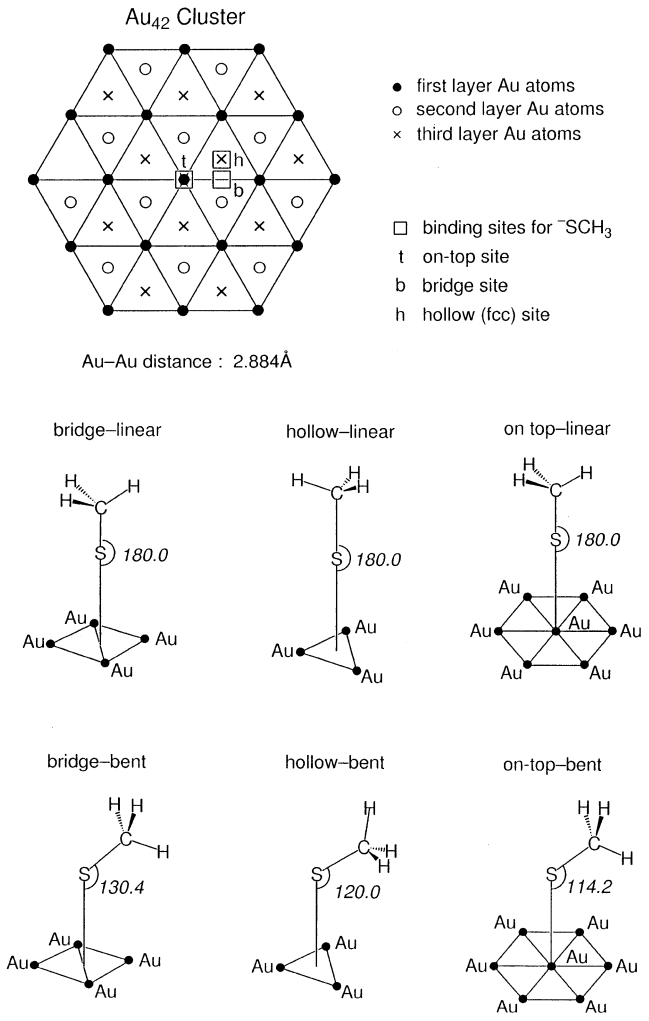

Figure 4. Au_{42} cluster and the structure of the SCH_3 part in each model. The geometrical parameters are identical to those presented in Figure 2 except the binding site−S−C angles in the bridge−linear, hollow−bent, and on-top−linear models.

of the S−C bonds. To see what orbitals of the Au surface participate in electron delocalization with $^-SCH_3$, we have carried out a paired interaction orbital analysis for the system consisting of a cluster of 42 Au atoms and $^-SCH_3$, as illustrated in Figure 4. We considered six kinds of adsorption models, namely, bridge−linear, bridge−bent, hollow−linear, hollow−bent, on-top−linear, and on-top−bent. The geometrical parameters are identical to those shown in Figure 2 except the binding site−S−C angles in the bridge−linear, hollow−bent, and on-top−linear models. For the hollow model, only the result on the *fcc* type adsorption is presented, because the bonding natures of the *fcc* and *hcp* models are essentially identical by the COOP and COHP analyses described above and also in the present FMO analysis. The nearest Au−Au distance was fixed to be 2.884 Å, and one Au atom in the third layer has been deleted to create a closed shell system. Then, we obtain 231 occupied molecular orbitals (MOs) and 147 unoccupied MOs for the Au_{42} cluster in the extended Hückel MO scheme. The approaching anion has seven occupied MOs and four unoccupied MOs. Electron delocalization takes place between the occupied MOs of one part and the unoccupied MOs of the other part.

Consider an interaction between the occupied MO ϕ_i of one fragment, say A, and the unoccupied MO ψ_l of the other part, say B. The interaction gives rise to two orbitals of the composite system, A−B. Assuming that the occupied MO ϕ_i is located lower in energy than the MO ψ_l, the occupied MO of A−B is given by

$$\Phi_l = c_i\phi_i + c_l\psi_l, \text{ with } |c_i| > |c_l| \tag{3}$$

When the interaction between the two fragments is weak, c_i and c_l are given by

$$c_i \cong 1 \tag{4}$$

$$c_l \cong \frac{H_{il} - S_{il}H_{ii}}{H_{ii} - H_{ll}} \tag{5}$$

in which

$$H_{ii} = \int \phi_i H \phi_i \, d\nu,\ H_{ll} = \int \psi_l H \psi_l \, d\nu,\quad H_{il} = \int \phi_i H \psi_l \, d\nu$$
$$S_{il} = \int \phi_i \psi_l \, d\nu \tag{6}$$

The strength of interaction and the energy gap between the two orbitals are represented by the numerator and the denominator of eq 5, respectively. The sign of c_l in eq 3 depends on the sign of c_i. Accordingly, the product of two coefficients c_ic_l can be a measure of the interaction between the two orbitals.

Each MO of the composite system of two fragments is given in the extended Hückel MO calculation by a linear combination of the AOs of the fragments. Then, the MO Φ_f of A−B can be rewritten in terms of a linear combination of the occupied and unoccupied MOs of the two fragments

$$\Phi_f = \sum_{i=1}^{m} c_{fi}\phi_i + \sum_{j=m+1}^{M} c_{fj}\phi_j + \sum_{k=1}^{n} c_{fk}\psi_k + \sum_{l=n+1}^{N} c_{fl}\psi_l \tag{7}$$

where ϕ_i (i = 1, 2, ..., m) and ϕ_j ($j = m + 1, m + 2, ..., M$) denote respectively the occupied and unoccupied canonical MOs of the fragment A and ψ_k (k = 1, 2, ..., n) and ψ_l ($l = n+1, n+2, ..., N$) indicate respectively the occupied and unoccupied MOs of the fragment B. This is our fragment molecular orbital (FMO) scheme.[42] We may take P_{il} defined by eq 8 as the measure of interaction between the occupied MO ϕ_i of A and the unoccupied MO ψ_l of B in the interacting system, A−B.[43]

$$P_{il} = 2\sum_{f=1}^{m+n} c_{fi}c_{fl} \tag{8}$$

Electron delocalization from $^-SCH_3$ to the Au cluster is represented by 7 × 147 orbital interactions in the extended Hückel canonical MO representation. Now, let us carry out simultaneous transformations of the fragment MOs within the occupied MO space of $^-SCH_3$ and within the unoccupied MO space of the Au cluster by diagonalizing $\mathbf{P}^\dagger\mathbf{P}$, the ($i$, l) element of $\mathbf{P}$ being P_{il}.[44] The purpose of doing the orbital transformations is to represent electron delocalization compactly in terms of pairs of interaction orbitals ϕ'_i and ψ'_l, the former being given by a linear combination of the occupied MOs ϕ_i of $^-SCH_3$ and the latter by a linear combination of the unoccupied MOs ψ_l of the Au cluster. That is, we try to reduce 7 × 147 orbital interactions to the interactions of seven paired orbitals (ϕ'_i; ψ'_i), $i, l = f = 1-7$.[45] The remaining 140 unoccupied orbitals of the cluster then do not find their optimum occupied counterparts in the attacking anion and, accordingly, do not participate significantly in electron delocalization. One will find shortly that the description of interaction is simpler, being well-represented by still fewer orbital pairs. Delocalization of electrons from the Au cluster to $^-SCH_3$ has been represented

by 231 × 4 orbital pairs in the canonical MO scheme and four orbital pairs in our scheme. Interactions in these orbital pairs have been shown, however, to be negligibly weak, compared to electron delocalization from the latter to the former.

The MOs of A−B are now represented in terms of the transformed occupied and unoccupied orbitals of the two fragments, some of which participate in the bonding between the fragments by making orbital pairs and some of which do not contribute significantly to the bonding, being unpaired

$$\Phi_f = \sum_{i=1}^{m} d_{fi}\phi'_i + \sum_{j=m+1}^{M} d_{fj}\phi'_j + \sum_{k=1}^{n} d_{fk}\psi'_k + \sum_{l=n+1}^{N} d_{fl}\psi'_l \quad (9)$$

Then, the contribution of the orbital pair (ϕ'_i; ψ'_l) to the total energy E of the composite system A−B is given by

$$E_{il} = 4\sum_{f=1}^{m+n} d_{fi}\mathrm{d}_{fl}\mathrm{H}'_{il} = 2P'_{il}\mathrm{H}'_{il} \quad (10)$$

where

$$H'_{il} = \int \phi'_i \mathrm{H}\psi'_l \,\mathrm{d}\nu \quad (11)$$

$$P'_{il} = 2\sum_{f=1}^{m+n} d_{fi}\mathrm{d}_{fl} \quad (12)$$

The total energy consists not only of the orbital interactions between the two fragments but also of the energies of paired and unpaired orbitals and the repulsive interactions between the occupied MOs of the two fragments. Contribution of orbital interaction in each pair of interacting orbitals to the change in energy ΔE upon the interaction between the two fragments is given by eq 13, under the assumption that the interaction is not yet strong

$$\Delta\mathrm{E}_{il} \cong \frac{2(H'_{il} - S'_{il}\mathrm{H}'_{ii})^2}{H'_{ii} - H'_{ll}} \quad (13)$$

It turns out that the matrix element $|H'_{il} - S'_{il}H'_{ii}|$ is not very small, relative to $|H'_{ii} - H'_{ll}|$, in the systems under consideration. Then, ΔE_{il} may be evaluated by subtracting $2H'_{ii}$ from the twice of the lower eigenvalue of the following 2 × 2 secular equations

$$\begin{vmatrix} H'_{ii} - \epsilon & H'_{il} - S'_{il}\epsilon \\ H'_{il} - S'_{il}\epsilon & H'_{ll} - \epsilon \end{vmatrix} = 0 \quad (14)$$

3.2. Results and Discussion. Table 4 presents the matrix elements for the six types of interactions between $^{-}SCH_3$ and the Au cluster, bridge−linear, bridge−bent, hollow−linear, hollow−bent, on-top−linear, and on-top−bent.[46] Pairs of orbitals participating significantly in electron delocalization from the $^{-}SCH_3$ part to the Au_{42} part in the bridge−bent, hollow−linear, and on-top−bent models (the favored structure for each binding site) are illustrated in Figures 5−7. The unoccupied interaction orbital of the cluster is shown above and the occupied counterpart of $^{-}SCH_3$ is given below in each pair. One finds that the orbital of the cluster is localized on several Au atoms around the reaction site and overlaps in-phase with the paired orbital of $^{-}SCH_3$. Four Au atoms on the first layer dominate electron delocalization in the bridge model, whereas three Au atoms play dominant roles in the hollow model. In the hollow model, the orbitals of two π-type lone pair of electrons on $^{-}SCH_3$ interact with the s-type AOs of the Au surface, giving rise to two strong pairs of interaction orbitals, pairs 1 and 2, as illustrated in Scheme 2. On the other hand, the σ-type lone-pair orbital interacts with the p-type AOs of the surface in pair 3. Pairs 1−3 correspond to types 1−3 AO interactions of the hollow model in Figure 3, respectively. It is interesting to see that the Au atoms in the second layer participate to some extent in the interaction in pair 3. The major components of the surface orbitals are the Au 6s and 6p AOs, with a concomitant mixing of the 5d AOs.[47] Thus, the results of the FMO analysis are very similar to those of the COOP and COHP analyses.

TABLE 4: Some Integrals Estimating the Contributions of the Pairs of Orbitals to Electron Delocalization from $^{-}SCH_3$ to the Au Surface (in eV)

type of interactions	pair 1	pair 2	pair 3	pair 4
bridge−linear				
$(H'_{il} - S'_{il}H'_{ii})$[a]	−0.917	−1.092	−1.616	−0.828
$(H'_{ll} - H'_{ii})$	2.049	2.670	5.305	13.174
bridge−bent				
$(H'_{il} - S'_{il}H'_{ii})$	−1.443	−1.339	−1.041	−0.654
$(H'_{ll} - H'_{ii})$	3.010	2.672	5.229	12.010
hollow−linear				
$(H'_{il} - S'_{il}H'_{ii})$	−1.263	−1.466	−1.707	−0.882
$(H'_{ll} - H'_{ii})$	1.955	3.337	5.070	12.675
hollow−bent by 60°				
$(H'_{il} - S'_{il}H'_{ii})$	−1.333	−1.071	−1.620	−0.587
$(H'_{ll} - H'_{ii})$	2.634	2.253	5.953	9.477
on-top−linear				
$(H'_{il} - S'_{il}H'_{ii})$	−2.255	−0.271	−0.247	−0.636
$(H'_{ll} - H'_{ii})$	7.041	1.251	1.451	13.708
on-top−bent				
$(H'_{il} - S'_{il}H'_{ii})$	−1.478	−1.520	−0.626	−0.206
$(H'_{ll} - H'_{ii})$	3.563	3.790	7.147	8.627

[a] The subscript i denotes the occupied interaction orbital of $^{-}SCH_3$ and l signifies the paired unoccupied counterpart of the Au Cluster. In pair f, $i = l = f$.

SCHEME 2

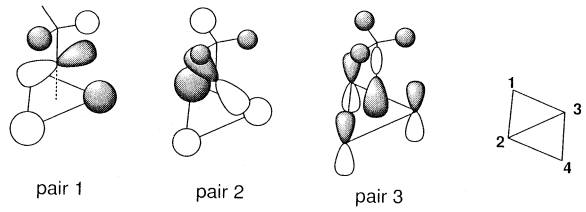

Calculations presented above reveal that $^{-}SCH_3$ prefers to coordinate to the Au surface vertical to the first layer in the hollow model and bent in other two models. The essence of the orbital interactions detected in the hollow model are illustrated in Scheme 2. In all of these three pairs, electron delocalization takes place from the $^{-}SCH_3$ fragment to the surface. Pairs 1 and 2 should be degenerate on the infinite surface. Tilting of the S−C bond leads to a significant weakening of orbital interactions as a consequence of loss of local C_{3v} symmetry. In pair 1, the hydrogen AOs come to overlap out-of-phase with the orbitals of the 6s AOs of Au2 and Au3. In the bent structure, the hydrogen AOs overlap in-phase with the AOs of the Au4 both in pair 2 and in pair 3. However, the interactions between the σ-type lone-pair orbital of S and the 6p AOs of Au2 and Au3 are weakened in pair 3, as represented by a decrease in the matrix element $|H'_{il} - S'_{il}H'_{ii}|$ by ∼ 0.09 eV upon the tilting of the S−C bond by 60°. The calculated values of stabilization brought about by electron delocalization in each orbital pair are presented in Table 5. The loss of the local symmetry results in a destabilization of the hollow model.

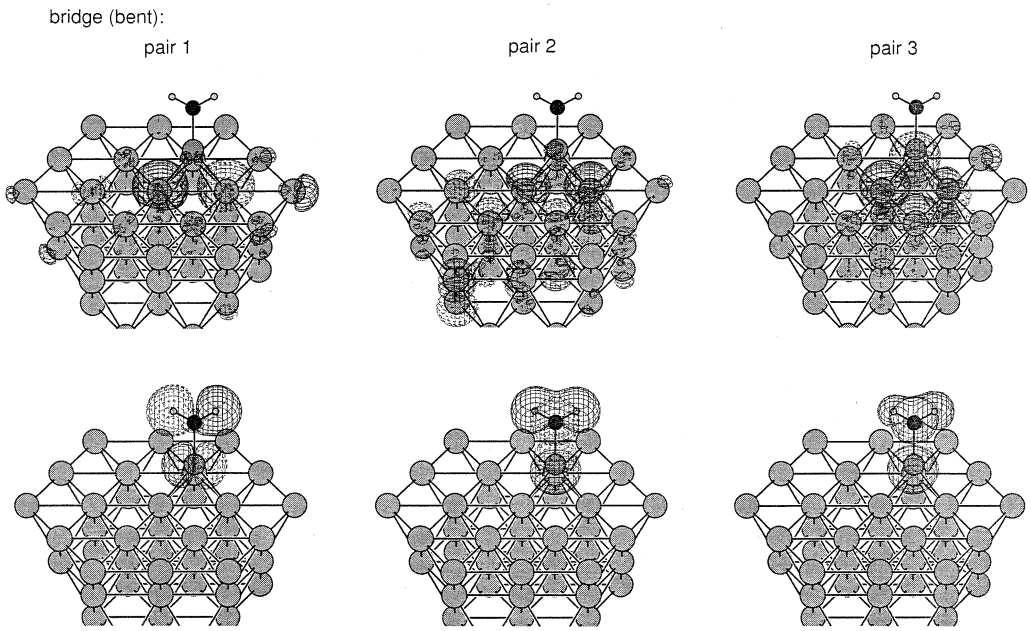

Figure 5. Pairs of orbitals participating significantly in electron delocalization from the $^{-}SCH_3$ part to the Au_{42} part in the bridge−bent model. The unoccupied interaction orbital of the cluster is shown above and the occupied counterpart of $^{-}SCH_3$ is given below in each pair.

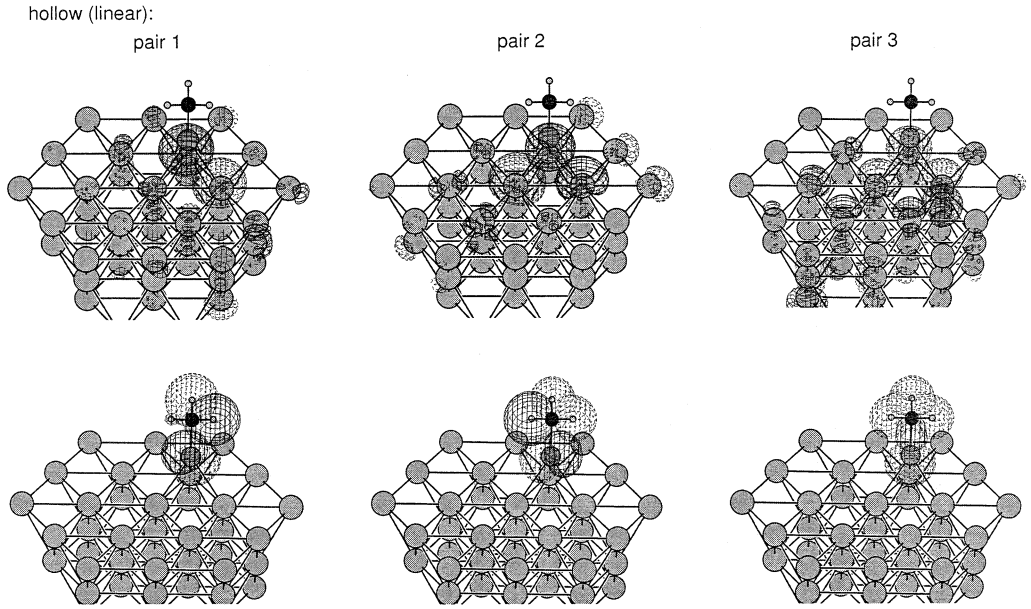

Figure 6. Pairs of orbitals participating significantly in electron delocalization from the $^{-}SCH_3$ part to the Au_{42} part in the hollow(*fcc*)−linear model. The unoccupied interaction orbital of the cluster is shown above and the occupied counterpart of $^{-}SCH_3$ is given below in each pair.

When $^{-}SCH_3$ coordinates vertical to the surface in the bridge model, orbital interactions illustrated in Scheme 3 play dominant roles in electron delocalization. The interactions in pair 1 and pair 2 are very similar to each other. The orbitals for the π-type lone pairs of electrons interact with the surface orbitals localized on the four nearest Au atoms. On the other hand, the σ-type lone pairs of electrons interact with the hybrids of s and p AOs on Au2 and Au3 in pair 3.

In the bent structure, the three pairs of interaction orbitals illustrated in Scheme 4 play dominant roles in electron delocalization. The π-type lone pairs of electrons of $^{-}SCH_3$ delocalize effectively to the s AOs of Au2 and Au3 in pair 1. The interaction in pair 1 has been shown to be stronger than that for the vertical coordination. Interestingly, the analysis shows that the σ- and π-type lone-pair orbitals rehybridize on S upon tilting. Then, the AOs of Au2 and Au3, mostly the 6s, get involved in bonding interactions with one of the lone pairs of electrons on S in pair 2. There is an H−Au secondary orbital interaction in this pair, leading to a strengthening of interaction upon tilting of the S−C bond. The hybrid orbital of the other lone pair of electrons overlaps in-phase with the mixture of the s- and p-type AOs of Au2 and Au3 in pair 3. This hybrid orbital overlaps in-phase with the p-type AO on Au1, but the interaction is not strong. An s-type AO of Au4 participates in the bonding interaction with the back lobe of the lone-pair orbital, but it interacts also with one of the methyl hydrogens in an antibonding fashion. Thus, the contribution of pair 3 to the S−Au bonding is weaker in the bent structure. Pairs 1 and 2 of Scheme 4 are related to types 2 and 1 AO interactions in Figure 3, respectively, although pair 3 cannot find its counterpart. Local symmetries are also seen in the paired orbitals of the bridge model.

In the vertical structure of the on-top model, the $^{-}SCH_3$ fragment has been shown to interact for the most part with the

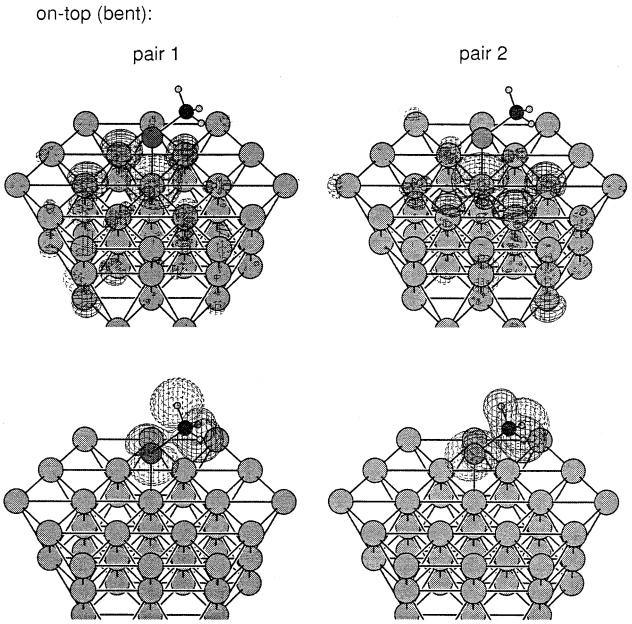

Figure 7. Pairs of orbitals participating significantly in electron delocalization from the $^{-}SCH_3$ part to the Au_{42} part in the on-top−bent model. The unoccupied interaction orbital of the cluster is shown above and the occupied counterpart of $^{-}SCH_3$ is given below in each pair.

TABLE 5: Contributions of Orbital Interactions to the Energy Change in the Interaction between $^{-}SCH_3$ and Au Cluster (in eV)

	ΔE_{il} [a]			
coordination type	pair 1	pair 2	pair 3	pair 4
bridge−linear				
$^{-}SCH_3 \rightarrow Au_{42}$	−0.640	−0.704	−0.811	−0.10
$Au_{42} \rightarrow {}^{-}SCH_3$	−0.005			
bridge−bent				
$^{-}SCH_3 \rightarrow Au_{42}$	−1.007	−0.987	−0.383	−0.07
$Au_{42} \rightarrow {}^{-}SCH_3$	−0.027			
hollow−linear				
$^{-}SCH_3 \rightarrow Au_{42}$	−1.075	−0.961	−0.923	−0.12
$Au_{42} \rightarrow {}^{-}SCH_3$	−0.013			
hollow−bent by 60°				
$^{-}SCH_3 \rightarrow Au_{42}$	−0.971	−0.776	−0.741	−0.07
$Au_{42} \rightarrow {}^{-}SCH_3$	−0.083			
on-top−linear				
$^{-}SCH_3 \rightarrow Au_{42}$	−1.126	−0.110	−0.080	−0.05
$Au_{42} \rightarrow {}^{-}SCH_3$	−0.104			
on-top−bent				
$^{-}SCH_3 \rightarrow Au_{42}$	−0.949	−0.951	−0.109	−0.01
$Au_{42} \rightarrow {}^{-}SCH_3$	−0.024			

[a] In the *f*th pair, *i* and *l* are *f*.

SCHEME 3

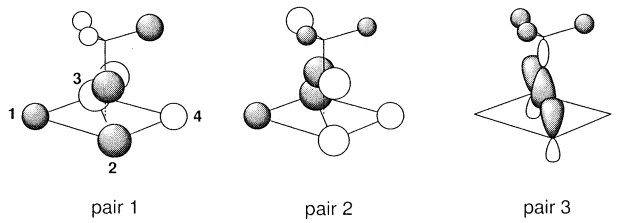

Au atom in the center of a hexagon. Orbital interactions cannot be strong in that structure, and stabilization is achieved by tilting the $^{-}SCH_3$ fragment. The bending angle should be larger in the on-top model than in the bridge model. Pair 1 of Figure 7 corresponds to the type 1 AO interaction in Figure 3.

SCHEME 4

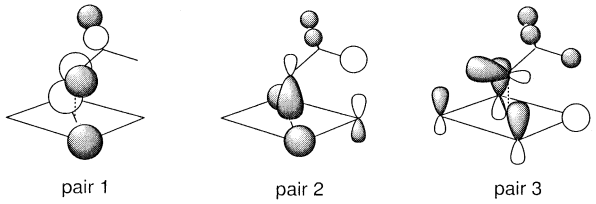

The present FMO analysis indicates that electron delocalization between $^{-}SCH_3$ and the Au cluster gets weaker in the order, hollow (linear) > bridge (bent) > on-top (bent). We have three pairs of strong orbital interactions in the hollow model. The overall features of the FMO results agree well with the results of the COOP and COHP analyses. Although there are some discrepancies, they could be reasonably attributed to the different models and methods of analysis.

4. Concluding Remarks

With the aid of crystal orbital overlap population (COOP) and crystal orbital Hamilton population (COHP) analyses for the three-layer slab models and fragment molecular orbital (FMO) analyses for the Au_{42} cluster model, we discuss the S−Au(111) bonding in the methanethiolate/Au(111) monolayer systems. We explain the origin of the S-surface bonding and the binding site preference from the viewpoint of orbital interactions. The site preference for methanethiolate adsorption is in the order of three-fold hollow (*fcc* and *hcp*) > bridge > on-top. The contribution of 5d(Au) orbitals to the S-surface bonding is small. The *fcc* and *hcp* adsorptions are almost identical in energy and S-surface bonding character, which demonstrates that the second-layer Au atoms have little influence on the S−Au(111) bonding. Although σ-character is dominant in the on-top model, π-type interactions contribute significantly to the S-surface bonding in the bridge and the hollow models. In particular, degenerate π-type interactions play important roles in the hollow models and are maximized when S−CH_3 is upright. FMO results explain well the vertical S−C bonds in the hollow models and the tilting S−C bonds in the on-top and bridge models.

Acknowledgment. K.Y. acknowledges the Ministry of Culture, Sports, Science and Technology of Japan, the Japan Society for the Promotion of Sciences, the Iwatani Naoji Foundation, the Takeda Science Foundation, and Kyushu University P & P "Green Chemistry" for their support of this work. This work was also supported by NSF Research Grant CHE 99-70089 to R.H. Computations were in part carried out at the Computer Center of the Institute for Molecular Science.

References and Notes

(1) (a) Nuzzo, R. G.; Allara, D. L. *J. Am. Chem. Soc.* **1983**, *105*, 4481. (b) Swalen, J. D.; Allara, D. L.; Andrade, J. D.; Chandross, E. A.; Garoff, S.; Israelachvili, J.; McCarthy, T. J.; Murray, R.; Pease, R. F.; Rabolt, J. F.; Wynne, K. J.; Yu, H. *Langmuir* **1987**, *3*, 932. (c) Bain, C. D.; Troughton, E. B.; Tao, Y.-T.; Evall, J.; Whitesides, G. M.; Nuzzo, R. G. *J. Am. Chem. Soc.* **1989**, *111*, 321. (d) Ulman, A. *An Introduction to Ultrathin Organic Films*; Academic Press: New York, 1991. (e) Ulman, A. *Chem. Rev.* **1996**, *96*, 1533. (f) Bumm, L. A.; Arnold, J. J.; Cygan, M. T.; Dunbar, T. D.; Burgin, T. P.; Jones, L., II.; Allara, D. L.; Tour, J. M.; Weiss, P. S. *Science* **1996**, *271*, 1705. (g) Maboudian, R. *Surf. Sci. Rep.* **1998**, *30*, 207. (h) Mitsuya, M.; Sato, N. *Langmuir* **1999**, *15*, 2099. (i) Ishida, T.; Mizutani, W.; Choi, N.; Akiba, U.; Fujihira, M.; Tokumoto, H. *J. Phys. Chem. B* **2000**, *104*, 11680. (j) Liu, G.-Y.; Xu, S.; Qian, Y. *Acc. Chem. Res.* **2000**, *33*, 457. (k) Giancarlo, L. C.; Flynn, G. W. *Acc. Chem. Res.* **2000**, *33*, 491.

(2) (a) Dubois, L. H.; Nuzzo, R. G. *Annu. Rev. Phys. Chem.* **1992**, *43*, 437. (b) Poirier, G. E. *Langmuir* **1997**, *13*, 2019. (c) Poirier, G. E. *Chem. Rev.* **1997**, *97*, 1117.

(3) (a) Poirier, G. E.; Pylant, E. D. *Science* **1996**, *272*, 1145. (b) Arce, F. T.; Vela, M. E.; Salvarezza, R. C.; Arvia, A. J. *J. Chem. Phys*. **1998**, *109*, 5703. (c) Kondoh, H.; Kodama, C.; Nozoye, H. *J. Phys. Chem. B* **1998**, *102*, 2310. (d) Kondoh, H.; Kodama, C.; Sumida, H.; Nozoye, H. *J. Chem. Phys*. **1999**, *111*, 1175. (e) Poirier, G. E. *Langmuir* **1999**, *15*, 1167.

(4) (a) Nuzzo, R. G.; Fusco, F. A.; Allara, D. L. *J. Am. Chem. Soc*. **1987**, *109*, 2358. (b) Porter, M. D.; Bright, T. B.; Allara, D. L.; Chidsey, C. E. D. *J. Am. Chem. Soc*. **1987**, *109*, 3559. (c) Bain, C. D.; Biebuyck, H. A.; Whitesides, G. M. *Langmuir* **1989**, *5*, 723. (d) Biebuyck, H. A.; Bain, C. D.; Whitesides, G. M. *Langmuir* **1994**, *10*, 1825.

(5) Nuzzo, R. G.; Zegarski, B. R.; Dubois, L. H. *J. Am. Chem. Soc*. **1987**, *109*, 733.

(6) Strong, L.; Whitesides, G. M. *Langmuir* **1988**, *4*, 546.

(7) Chidsey, C. E. D.; Loiacono, D. N. *Langmuir* **1990**, *6*, 682.

(8) Samant, M. G.; Brown, C. A.; Gordon, J. G., II. *Langmuir* **1991**, *7*, 437.

(9) Hautman, J.; Klein, M. L. *J. Chem. Phys.* **1990**, *93*, 7483.

(10) Widrig, C. A.; Alves, C. A.; Porter, M. D. *J. Am. Chem. Soc*. **1991**, *113*, 2805.

(11) Ogletree, D. F.; Ocal, C.; Marchon, B.; Somorjai, G. A.; Salmeron, M.; Beebe, T.; Siekhaus, W. *J. Vac. Sci. Technol. A* **1990**, *8*, 297. (b) Camillone, N., III.; Chidsey, C. E. D.; Liu, G.-Y.; Scoles, G. *J. Chem. Phys*. **1993**, *98*, 4234. (c) Mar, W.; Klein, M. L. *Langmuir* **1994**, *10*, 188.

(12) Ishida, T.; Yamamoto, S.; Mizutani, W.; Motomatsu, M.; Tokumoto, H.; Hokari, H.; Azehara, H.; Fujihira, M. *Langmuir* **1997**, *13*, 3261.

(13) Noh, J.; Hara, M. *Langmuir* **2000**, *16*, 2045.

(14) Camillone, N., III.; Chidsey, C. E. D.; Liu, G.-Y.; Scoles, G. *J. Chem. Phys*. **1993**, *98*, 3503.

(15) Fenter, P.; Eisenberger, P.; Liang, K. S. *Phys. Rev. Lett.* **1993**, *70*, 2447.

(16) Fenter, P.; Schreiber, F.; Berman, L.; Scoles, G.; Eisenberger, P.; Bedzyk, M. J. *Surf. Sci*. **1998**, *412/413*, 213.

(17) (a) Bucher, J. P.; Santesson, L.; Kern, K. *Appl. Phys. A* **1994**, *59*, 135. (b) Delamarche, E.; Michel, B.; Gerber, Ch.; Anselmetti, D.; Güntherodt, H.-J.; Wolf, H.; Ringsdorf, H. *Langmuir* **1994**, *10*, 2869. (c) Poirier, G. E.; Tarlov, M. J. *Langmuir* **1994**, *10*, 2853. (d) Barrena, E.; Ocal, C.; Salmeron, M. *J. Chem. Phys*. **1999**, *111*, 9797.

(18) Fenter, P.; Eberhardt, A.; Eisenberger, P. *Science* **1994**, *266*, 1216.

(19) Yeganeh, M. S.; Dougal, S. M.; Polizzotti, R. S.; Rabinowitz, P. *Phys. Rev. Lett*. **1995**, *74*, 1811.

(20) Kluth, G. J.; Carraro, C.; Maboudian, R. *Phys. Rev. B* **1999**, *59*, 10449(R).

(21) Gerdy, J. J.; Goodard, W. A., III. *J. Am. Chem. Soc*. **1996**, *118*, 3233.

(22) Sellers, H.; Ulman, A.; Shnidman, Y.; Eilers, J. E. *J. Am. Chem. Soc*. **1993**, *115*, 9389.

(23) (a) Beardmore, K. M.; Kress, J. D.; Bishop, A. R.; Grønbech-Jensen, N. *Synth. Met*. **1997**, *84*, 317. (b) Beardmore, K. M.; Kress, J. D.; Grønbech-Jensen, N.; Bishop, A. R. *Chem. Phys. Lett*. **1998**, *286*, 40.

(24) Häkkinen, H.; Barnett, R. N.; Landman, U. *Phys. Rev. Lett*. **1999**, *82*, 3264.

(25) Grönbeck, H.; Curioni, A.; Andreoni, W. *J. Am. Chem. Soc*. **2000**, *122*, 3839.

(26) Hayashi, T.; Morikawa, Y.; Nozoye, H. *J. Chem. Phys*. **2001**, *114*, 7615.

(27) Vargas, M. C.; Giannozzi, P.; Selloni, A.; Scoles, G. *J. Phys. Chem. B* **2001**, *105*, 9509.

(28) Yourdshahyan, Y.; Zhang, H. K.; Rappe, A. M. *Phys. Rev. B* **2001**, *63*, 081405(R).

(29) (a) Pyykkö, P. *Chem. Rev*. **1988**, *88*, 563. (b) Bond, G. C.; Thompson, D. T. *Catal. Rev. Sci. Eng*. **1999**, *41*, 319. (c) Bond, G. C. *J. Mol. Catal. A. Chem.* **2000**, *156*, 1.

(30) Akinaga, Y.; Nakajima, T.; Hirao, K. *J. Chem. Phys*. **2001**, *114*, 8555.

(31) Gottschalck, J.; Hammer, B. *J. Chem. Phys*. **2002**, *116*, 784.

(32) (a) Hoffmann, R.; Lipscomb, W. N. *J. Chem. Phys.* **1962**, *36*, 2179; *37*, 2872. (b) Hoffmann, R. *J. Chem. Phys.* **1963**, *39*, 1397. (c) Hoffmann, R. *J. Chem. Phys.* **1964**, *40*, 2474, 2745.

(33) (a) Hoffmann, R. *Solids and Surfaces: A Chemist's View of Bonding in Extended Structures*; VCH Publishers: New York, 1988. (b) Hughbanks, T.; Hoffmann, R. *J. Am. Chem. Soc*. **1983**, *105*, 3528. (c) Saillard, J.-Y.; Hoffmann, R. *J. Am. Chem. Soc*. **1984**, *106*, 2006.

(34) (a) Dronskowski, R.; Blöchl, P. E.; *J. Phys. Chem.* **1993**, *97*, 8617. (b) Glassey, W. V.; Papoian, G. A.; Hoffmann, R. *J. Chem. Phys.* **1999**, *111*, 893. (c) Papoian, G.; Nørskov, J. K.; Hoffmann, R. *J. Am. Chem. Soc*. **2000**, *122*, 4129.

(35) Hoffmann, R.; Albright, T. A.; Thorn, D. L. *Pure Appl. Chem*. **1981**, *50*, 1.

(36) (a) Harten, U.; Lahee, A. M.; Toennies, J. P.; Wöll, Ch. *Phys. Rev. Lett.* **1985**, *54*, 2619. (b) Wöll, Ch.; Chiang, S.; Wilson, R. J.; Lippel, P. H. *Phys. Rev. B* **1989**, *39*, 7988. (c) Sandy, A. R.; Mochrie, S. G. J.; Zehner, D. M.; Huang, K. G.; Gibbs, D. *Phys. Rev. B* **1991**, *43*, 4667.

(37) (a) Naidu, S. V. N.; Houska, C. R. *J. Appl. Phys*. **1971**, *42*, 4971. (b) Frenkel, A. I.; Machavariani, V. Sh.; Rubshtein, A.; Rosenberg, Yu.; Voronel, A.; Stern, E. A. *Phys. Rev. B* **2000**, *62*, 9364.

(38) (a) Becke, A. D. *Phys. Rev. A* **1988**, *38*, 3098; *J. Chem. Phys*. **1993**, *98*, 5643. (b) Lee, C.; Yang, W.; Parr, R. G. *Phys. Rev. B* **1988**, *37*, 785. (c) Stephens, P. J.; Devlin, F. J.; Chabalowski, C. F.; Frisch, M. J. *J. Phys. Chem.* **1994**, *98*, 11623.

(39) Delley, B. *J. Chem. Phys.* **1990**, *92*, 508.

(40) Wolfsberg, M.; Helmholz, L. *J. Chem. Phys*. **1952**, *20*, 837.

(41) Landrum, G. A.; Glassey, W. V. *YAeHMOP: Yet Another extended Hückel Molecular Orbital Package*; Cornell University: Ithaca, New York, 1995. http://sourceforge.net/projects/yaehmop/

(42) Fujimoto, H.; Hoffmann, R. *J. Phys. Chem.* **1974**, *78*, 1167.

(43) Other orbital effects, e.g., polarization, are also included in the coefficients.

(44) (a) Fujimoto, H.; Koga, N.; Fukui, K. *J. Am. Chem. Soc.* **1981**, *103*, 7452. (b) Fujimoto, H.; Yamasaki, T.; Mizutani, H.; Koga, N. *J. Am. Chem. Soc.* **1985**, *107*, 6157. (c) Fujimoto, H.; Yamasaki, T. *J. Am. Chem. Soc.* **1986**, *108*, 578. (d) Omoto, K.; Sawada, Y.; Fujimoto, H. *J. Am. Chem. Soc.* **1996**, *118*, 1750. (e) Omoto, K.; Fujimoto, H. *J. Am. Chem. Soc.* **1997**, *119*, 5366.

(45) Hereafter, the prime denotes the transformed orbitals and the quantities defined for those orbitals.

(46) We have deleted one Au atom in the third layer to avoid complicated arguments on spins. There arise then two choices in placing $^{-}SCH_3$ in each type of interaction, but the defect in the third layer has been shown to have little influence on the results of present analysis. This method can be extended in a straightforward manner to the interactions between closed-shells and open-shells and between two open-shells by carrying out the orbital transformations on the α spin part and on the β spin part, separately.

(47) The participation of the 5d AOs into the interaction orbitals of the Au surface is small, the square of coefficient being calculated to be less than 1/10 of that of the 6s AOs at the reaction centers.